Check for
updates

Direct Evidence for Magnetic Reconnection in a Solar EUV Nanoflare

Artem S. Ulyanov[1] · Sergey A. Bogachev[1] ·
Ivan P. Loboda[1] · Anton A. Reva[1] ·
Alexey S. Kirichenko[1]

Abstract We provide observational evidence that the mechanism of solar EUV nanoflares may be close to the standard flare model. The object of our study was a nanoflare on 25 February 2011, for which we determined a plasma temperature of 3.1 MK, a total thermal energy of 6.2×10^{25} erg, and an electric-current distribution that reaches its maximum at a height of ≈ 1.5 Mm. Despite the lack of spatial resolution, we reconstructed the 3D magnetic configuration for this event in the potential and non-linear force-free-field interpolations. As a result, we identified four null-points, two of which were coincident with the region of maximal energy release. The nanoflare was initiated by a new small-scale magnetic flux, which appeared on the photosphere about $15 - 20$ minutes before the nanoflare. The total free energy stored in the region before the nanoflare was $\approx 8.9 \times 10^{25}$ erg. Only about two-thirds of this amount was transferred into the plasma heating and EUV radiation. We posit that the remaining energy could be transferred during particle acceleration and plasma motions, which are still inaccessible for direct observations in nanoflares.

1. Introduction

The major radiation of solar corona lies in the extreme ultraviolet (EUV) part of the spectrum, which is not accessible for observation from the Earth's surface. The EUV spectrum of the corona consists mainly of emission lines of metals with high degrees of ionization, which correspond to temperatures of about 1 million K (MK). Images of the corona in these spectral lines obtained with space-borne telescopes (*Extreme ultraviolet Imaging Telescope* (EIT) onboard the *Solar and Heliospheric Observatory* (SOHO: Delaboudinière *et al.*, 1995), *Telescope-Spectrometer for Imaging Spectroscopy* (TeSIS) onboard the CORONAS-*Photon* spacecraft (Kuzin *et al.*, 2009), *Atmospheric Imaging Assembly* (AIA) onboard the

✉ S.A. Bogachev
bogachev@lebedev.ru

1   P.N. Lebedev Physical Institute of the Russian Academy of Sciences, 53 Leninskiy Prospekt, 119991, Moscow, Russia

Springer

Solar Dynamics Observatory (SDO: Lemen *et al.*, 2012), and others) demonstrate that, along with the large-scale structures, there are always many compact, point-like sources of EUV radiation in the corona with very short lifetimes; such times last from a few tens of seconds to several minutes (Hudson, 1991; Shimizu and Tsuneta, 1997), which cover the solar disk in a nearly random way. The total energy released in such radiation sources lies in the range $10^{24} - 10^{27}$ erg (Parnell and Jupp, 2000), which is equal to $10^{-9} - 10^{-6}$ of the energy of large solar flares. This is one of the reasons why these events are often called "nanoflares", a term introduced by Parker (1988).

The larger events (microflares and X-ray bright points), which can be observed in more detail, are usually explained as multiple small-scale events of plasma heating (Benz and Grigis, 2002; Reva *et al.*, 2012; Kirichenko and Bogachev, 2013; Barnes, Cargill, and Bradshaw, 2016b,a; Kirichenko and Bogachev, 2017a). Due to the short duration of the process, the heat flows cannot spread from the flare center into the neighboring areas, and the radiation source remains compact during the entire observation time. If we apply this model to nanoflares, we can assume that in events of this type, the heating process involves only a single small magnetic loop, or even a part of that loop. The size of the radiation source in this case should not exceed a few thousand kilometers [km], which corresponds to one or several pixels in up-to-date images of the Sun. For this reason, due to the insufficient spatial resolution of the present instrumentation, the structure of nanoflares and their mechanism are still not clearly determined.

The study of nanoflares is of particular interest in the context of the coronal-heating problem. It is known that the small-scale magnetic reconnection may be a possible mechanism that heats the solar corona (see, for example, Priest, 2014). The micro- and nanoflares may be considered as a visible manifestation of this reconnection process (Meyer, Mackay, and van Ballegooijen, 2012; Cranmer, 2018). In this case, they may provide quantitative information on whether the energy release during small-scale reconnection is sufficient to heat the corona or not (see, for example, Guerreiro *et al.*, 2017; Priest, Chitta, and Syntelis, 2018).

Despite the significant progress in the study of small-scale activity, the relation between micro- and nanoflares and magnetic reconnection is still not clear and is usually revealed indirectly. In solar microflares, for instance, the relation is known between their emissions and magnetic-flux values (Pevtsov *et al.*, 2003; Kirichenko and Bogachev, 2017b). Other studies have confirmed that the small-scale energy release is sometimes preceded by magnetic-flux cancellation or other morphological evidence for magnetic reconnection (Georgoulis *et al.*, 2002; Watanabe *et al.*, 2011; Reid *et al.*, 2016). A correlation has also been reported between bright magnetic points (small-scale concentrations of magnetic field near the solar surface; Stenflo, 1985) and the Ellerman bombs (short-lived events observed in the wings of the Hα line; *e.g.* Nelson *et al.*, 2013). However, most of these studies were based on statistical methods and did not attempt to resolve the specific magnetic structures that produced a particular event. The reason is that the magnetic features responsible for small-scale reconnection are usually very close to the resolution limit, and it is impossible to identify them without a significant uncertainty. As a result, the nature of solar nanoflares is not yet reliably confirmed.

In the present work, using solar EUV images in the 131 Å, 171 Å, and 193 Å channels of AIA telescopes and magnetograms from the *Helioseismic and Magnetic Imager* (HMI) onboard the SDO, we were able to find an isolated nanoflare for which the relationship between the energy release and the magnetic-field dynamics seems to be well established. A detailed study of this event showed that its origin and evolution were in good agreement with the standard model of a solar flare, according to which the energy release in the corona

results from the interaction and reconnection of magnetic flux of opposite polarities. We believe that this result strongly supports the assumption that at least some part of the energy release in the solar corona is driven by small-scale magnetic reconnection.

The layout of this article is as follows: In Section 2 we give an overview of the observational data utilized in the study and describe the methods employed to process them. This is followed by the results of the study, which are outlined in Section 3. Finally, in Section 4, we discuss the results.

2. Observations and Data Processing

The source of the data that we used in the article were the AIA and HMI instruments, both operating onboard the SDO spacecraft. AIA telescopes provide images of the full disk of the Sun with a high angular resolution of $0.6''$ per pixel at a cadence of about 12 seconds in seven EUV wavebands (Lemen *et al.*, 2012). For the purposes of this study, we used only images from three AIA channels: the 131 Å channel, the radiation in which is formed mainly by the Fe XX and Fe XXIII lines at a plasma temperature of ≈ 10 MK; the 171 Å channel dominated by the Fe IX line formed at $T \approx 0.7$ MK, and the 193 Å channel, in which the dominant ion, Fe XII, is formed at $T \approx 1.5$ MK. The identification of events was based mainly on the 171 Å data; the other two channels were used to eliminate errors and to analyze the spectral characteristics of the radiation.

The magnetograms from HMI were used to study the magnetic-field configuration in the region of the nanoflare. The corresponding images are maps of the normal component of the magnetic field (along the line of sight) measured at the level of the Sun's photosphere. The angular resolution of these observations is $0.5''$ per pixel at a cadence of approximately 45 seconds (Scherrer *et al.*, 2012).

For this study, we have chosen a six-hour interval starting at 00:00 UT on 25 February 2011 and ending at 06:00 UT of the same day. After that, an area of 512×512 pixels was selected on the solar disk. The selection criteria for the area were very simple. We avoided active regions with bright magnetic loops. Another important consideration was the absence of ordinary solar flares within the selected area (GOES class C1.0 and larger). In all other respects, the time of observation and the area on the solar disk were chosen randomly. The total number of processed images was 1800 in each channel, or 5400 in total for all three AIA channels. These data were processed to remove the background and to compensate for the differential rotation of the Sun. After this, every set of 1800 images for each channel was transformed into a data cube with dimensions $512 \times 512 \times 1800$. The three resulting data cubes were then used for scientific analysis.

The events (nanoflares) were detected in the data cubes as a group of adjacent pixels that exhibited a sharp burst of EUV radiation during a certain time interval with approximately the same temporal characteristics in all of the pixels. In more detail, our algorithm performed the following main steps:

  i) It automatically removes bright tracks produced by energetic particles.
 ii) It defines and subtracts the background component of the signal.
iii) It selects the statistically significant events.

In step i), we compared the signal from every pixel with its value measured in the next image. Then we chose the minimum value between these two subsequent readings and wrote it to the pixel. This fast method slightly distorted the signal but was effective in removing artifacts associated with charged particles.

In step ii), we divided the emission time profile measured in the pixel into three-minute segments. For the entire six-hour period, this gave us 120 time intervals. Then we derived the median value of the signal for every interval and obtained 120 points, which were then fitted by means of spline interpolation. We considered the resulting smooth curve as the background component for the signal from the specific pixel.

In step iii), we picked all of the readings that exceeded a threshold of 3σ above the background, where σ was the standard deviation of the signal. In order to enhance the accuracy of the analysis, the threshold can be increased to 5σ. In our experience, this completely eliminates false flares, but dramatically reduces the number of events. Finally, as we said above, we grouped the spikes detected in adjacent pixel into a single event.

Using this procedure, we pre-selected several hundred events, the largest of which had already been studied individually. Below, we describe in detail a nanoflare, for which we have found the most evident correlation between the energy release and the dynamics of the magnetic field. Since the goal of this article does not include a statistical analysis, we have not studied in detail all of the other events. Our analysis of the data shows that the largest nanoflares are usually clearly preceded by noticeable changes in the magnetic field. For the majority of the events, however, it is difficult to get any reliable conclusions because of the low level and complicated dynamics of the surrounding magnetic fields.

3. Results

The nanoflare and its nearest surroundings are shown in Figure 1. The figure contains four panels, three of which are the same frame of the solar disk obtained in the three AIA channels (131, 171, and 193 Å), and the last one is a magnetic-field map by HMI reduced to AIA scale. All of the images correspond approximately to the maximum EUV emission. The frames are squares with the dimensions of 64×64 AIA pixels ($\approx 38''$ or about 28 Mm). The compact source of radiation, which we identify as a nanoflare, was observed in the corona in all three channels and was associated with a compact loop system, which is also clearly visible in the images. The size of the flaring region defined by the distance between the loop footpoints was about 20 Mm. The brightest emissions were observed near the loop top, which is very similar to the classical picture of a solar flare, according to which the most intense radiation in the corona is formed near the top or just above the flaring loops (see, for example, Somov, 2007).

A more detailed presentation of the nanoflare evolution is given in Figure 2. The panels contain 6×4 snapshots obtained simultaneously in the 131, 171, and 193 Å channels of the AIA instrument as well as the corresponding magnetic maps from HMI. The top two panels in each row correspond to the pre-flare situation, the next two rows are obtained near the nanoflare maximum, and the last two give a post-flare view.

In order to obtain the radiation profiles of the nanoflare, we integrated the signal over the region of the most intense energy release in the 131, 171, and 193 Å AIA channels. The area of integration had a size of 8×8 AIA pixels and is shown in Figure 1 as a gray square in the top-left panel. Preliminarily, we ensured that the radiation source was in this area during the entire nanoflare lifetime. The result (time profiles of the nanoflare obtained in the three AIA channels) is shown in Figure 3.

The radiation profile of the nanoflare is rather complicated and looks more like a series of several recurrent events than a single event. The first, most powerful burst was observed between 01:35 UT and 01:44 UT and, accordingly, lasted about 9 minutes. It was accompanied by the second burst observed between 01:44 UT and 01:51 UT (7 minutes) and then
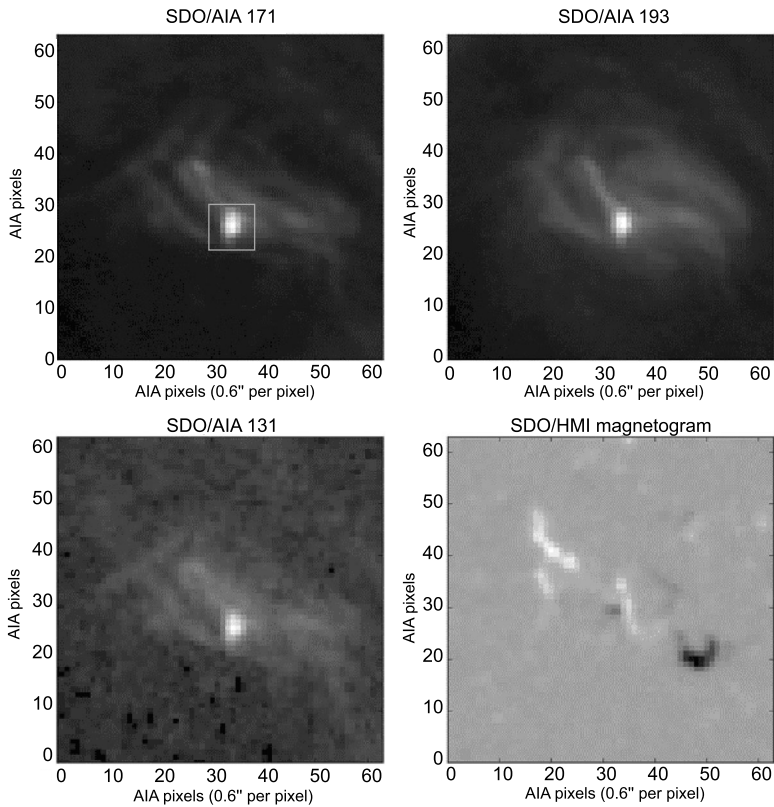
Figure 1 Simultaneous images of the nanoflare in the 171 Å (*top-left*), 131 Å (*bottom-left*), and 193 Å (*top-right*) AIA channels, and the corresponding HMI magnetogram (*bottom-right*). The *white square* in the *top-left panel* marks the region of the most intense energy release.

by the third one between 01:51 UT and 01:58 UT (7 minutes). From this, the total duration of the event was $25 - 30$ minutes. The phase of the most intense energy release (first burst) lasted about 10 minutes.

From Figure 3, every burst (especially the first one) may also be subdivided into smaller narrow spikes with a duration of about one minute. One possible explanation is that such a shape reproduces the real impulsive character of energy release in the event. We can refer to the observations of large solar flares, the hard X-ray profiles of which often consist of many elemental spikes (Hoyng, Brown, and van Beek, 1976). Such a picture is not typical for the EUV spectral range due to the strong influence of thermal emissions, which smooth the profiles. In the case of nanoflares, however, the bulk of the heated plasma is significantly less, and their EUV profiles can reproduce the non-thermal impulsive nature of energy release in more detail.

The plasma temperature near the nanoflare maximum was estimated by comparing the EUV emission in the 171 and 131 Å channels using the temperature response of the channels:

$$T\left(\frac{I_{131}}{I_{171}}\right) \approx 3.1 \text{ MK}. \tag{1}$$

Figure 2 Solar region, where the nanoflare took place, from SDO/AIA and SDO/HMI observations. *First three columns* are AIA 171 Å, 193 Å, and 131 Å channels, respectively; the *last column* contains HMI magnetograms. The images describe the temporal evolution of the nanoflare from its pre-flare stage (the *upper two rows* at 01:10 UT and 01:20 UT) through to the maximum energy release (01:36 UT and 01:37 UT) and up to the after-flare scenario (the *bottom two rows* at 02:00 UT and 05:00 UT). The field of view is 64×64 AIA pixels (≈ 28 Mm).
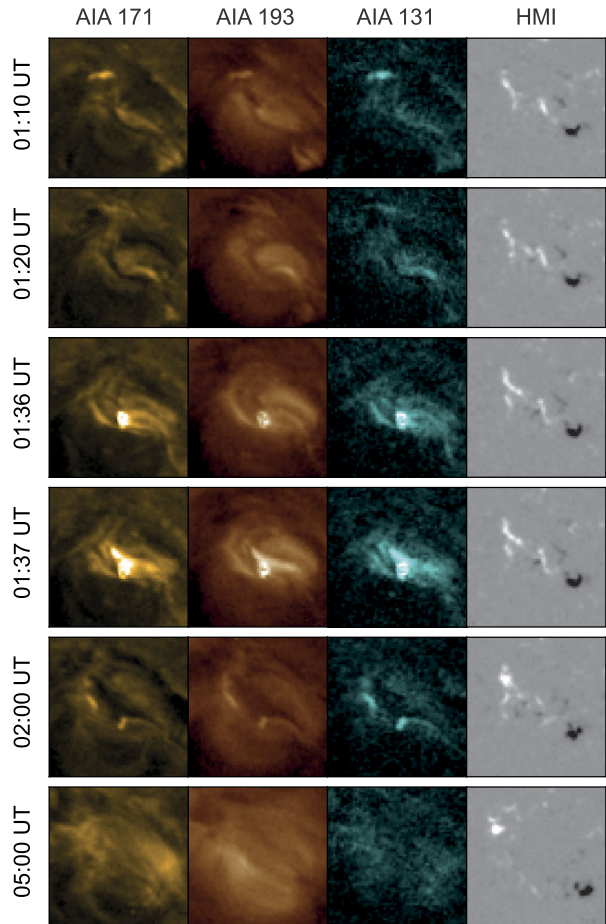
We consider this estimate to be correct because if the temperature were significantly higher, the radiation profile would have a long decay phase associated with plasma cooling. Note that the source that we have investigated was one of the brightest in our dataset. Therefore, we have deemed the temperature of 3 MK to be close to the upper limit for nanoflares.

Based on the plasma temperature, we estimated the amount of thermal energy released in the nanoflare as

$$E_{th} = 3 n_e k_B T V \approx 6.2 \times 10^{25} \text{ erg}, \tag{2}$$

where $k_B = 1.38 \times 10^{-16}$ erg K^{-1} is the Boltzmann constant; n_e is the electron number density, which was taken equal to 10^9 cm^{-3}, and T is the plasma temperature from Equation 1. The volume $[V]$ of the radiation source may be estimated as $V = Ah$, where A is the source area in the image and h is its thickness measured along the line of sight. The thickness h is unknown. Following some other articles (see, for example, Benz and Krucker, 2002) we set $h = \sqrt{A}$ and found $V = 4.8 \times 10^{25}$ cm^3. The resulting value of energy, 6×10^{25} erg, lies approximately in the middle of the energy range $10^{24} - 10^{27}$ erg, which usually relates to nanoflares (Aschwanden, 1999; Benz and Krucker, 2002).

Figure 3 Radiation profile of the nanoflare measured in three AIA channels: 131 Å (*dashed line*), 171 Å (*solid line*), and 193 Å (*dotted line*).
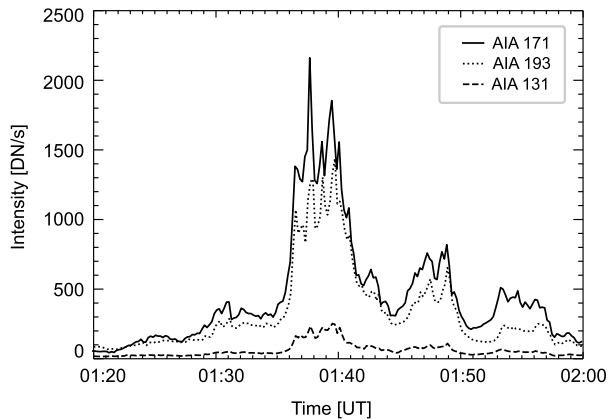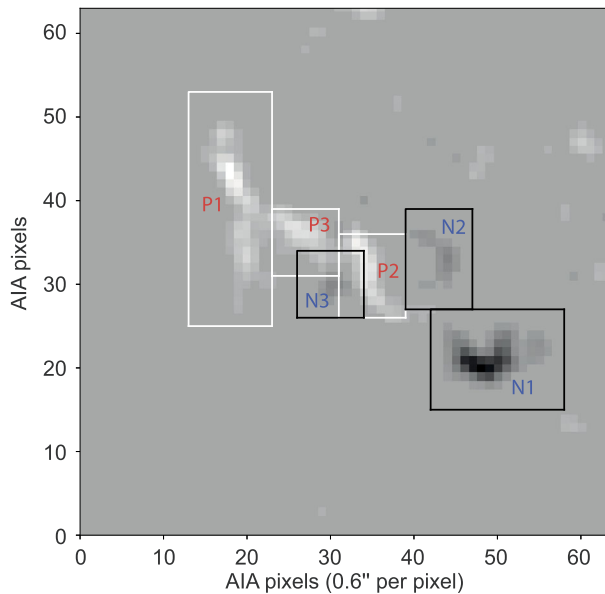

Figure 4 Distribution of magnetic fields on the Sun's surface during the maximum of the nanoflare EUV emission. The positive (P1 – P3) and negative (N1 – N3) magnetic polarities are outlined with *white* and *black rectangles*, respectively.

The configuration of the photospheric magnetic fields at the nanoflare maximum is shown in Figure 1 (lower-right panel). In Figure 4, we show its enlarged version with additional indication of the major magnetic fluxes. As P1, P2, and P3, we mark the fluxes of positive polarity (the magnetic field is oriented towards the observer), while N1, N2, and N3 are the negative polarity fields oriented away from the observer. According to Figure 2, the fluxes P3 and N3 did not exist in the pre-flare configuration (the upper HMI image on 01:10 UT) and appeared just before the nanoflare (next image: 01:20 UT). The post-flare configuration (last panel on 05:00 UT) already contains only two magnetic centers: P1 and N1. All of the other fluxes disappeared at this point. This shows that the magnetic configuration was not stable and had undergone a substantial transformation before and during the nanoflare.

To investigate the magnetic structure in more detail and to study its dynamics, we applied a well-known method based on imaginary magnetic "charges", which are placed under the surface of the Sun. The number, position, and values of these charges are adjusted in order

Figure 5 3D reconstruction of coronal magnetic fields for two different moments: 25 minutes before the nanoflare (01:10 UT; *top panel*) and 15 minutes before the nanoflare (01:20 UT; *bottom panel*). Symbols P1 – P3 and B1 – B3 are magnetic "charges" of positive and negative polarities; B1, A2, B3, and A4 are magnetic null-points located in the corona. *Solid lines* are magnetic separators, and *dashed lines* are the intersections of magnetic separatrices with the Sun's photosphere.
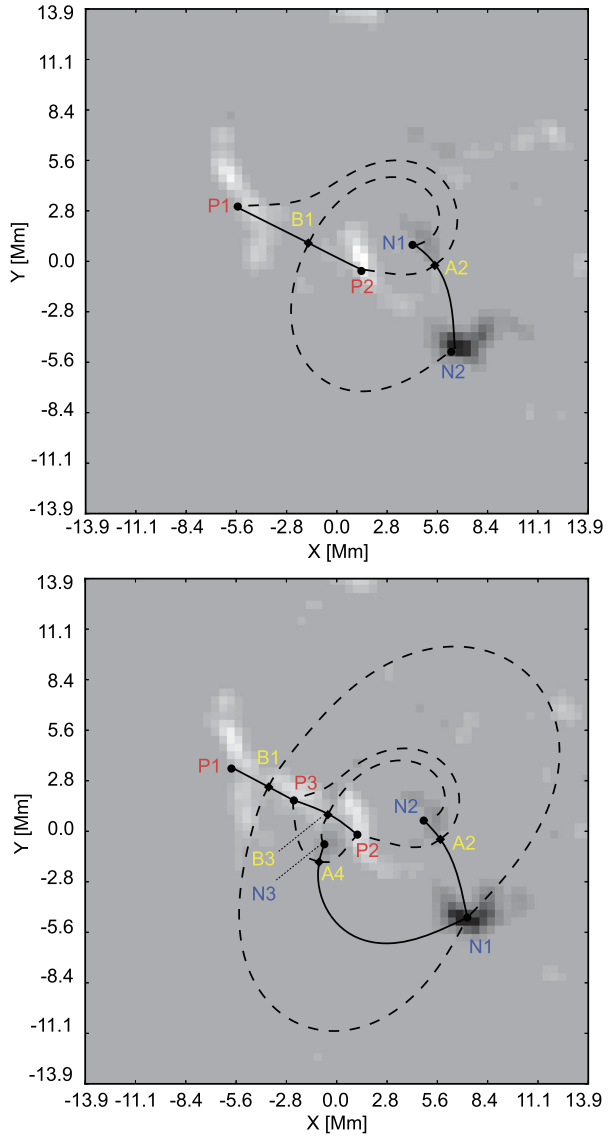

to achieve the best fit between the calculated and observed magnetic fields at the level of the photosphere. After we achieve such an adjustment at the photosphere, we can extrapolate the magnetic lines into the corona in order to reconstruct the 3D configuration of the potential magnetic field (Longcope, 2005):

$$\boldsymbol{B}(\boldsymbol{r}) = \sum_i \frac{q_i(\boldsymbol{r} - \boldsymbol{r}_i)}{|\boldsymbol{r} - \boldsymbol{r}_i|^3}, \tag{3}$$

where q_i is the magnetic charge, $\boldsymbol{r}_i$ is the charge position in a certain coordinate system, and $\boldsymbol{r}$ is an arbitrary point in the corona in the same coordinate system.

Figure 6 Transverse plasma motions at the Sun's surface during the nanoflare. The reconstruction is made by the DAVE method (Schuck, 2006). The background is a colorized magnetic map: positive polarities are *red*, and negative polarities are *blue*.
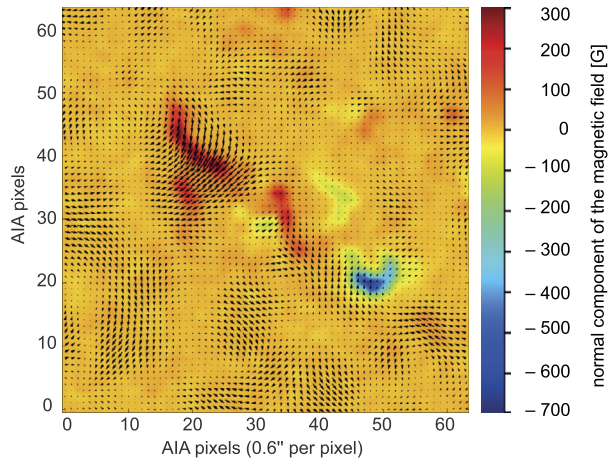
The results of such an investigation are shown in Figure 5. The top panel demonstrates the magnetic configuration on 01:10 UT (25 minutes before the nanoflare has occurred). The bottom panel is the same picture on 01:20 UT (15 minutes before the nanoflare). We mark in the pictures the following topological features: P1 – P3 and N1 – N3 are the magnetic "charges" of positive and negative polarities, respectively; dashed lines are the intersections of magnetic separatrices with the sun's surface; solid lines are the separators; and diamonds marked as B1, A2, B3, and A4 are the null-points of two different types. The most important difference between initial (top panel) and pre-flare (bottom panel) configurations is an emergence of new magnetic flux, P3 – N3, which creates two new null-points, B3 and A4. Just in the vicinity of these points there was the most intense energy release during the nanoflare (see for comparison Figure 1).

The emergence of the flux P3 – N3 and formation of null-points B3 and A4 had started approximately 15 – 20 minutes before the nanoflare maximum. This is consistent with the standard scenario, according to which solar flares should be preceded by the energy accumulation process, which may last several hours or more. If we apply this scenario to the nanoflare studied, we can conclude that the energy accumulation in this case took about 15 – 20 minutes. We, however, cannot be sure whether this time is typical for nanoflares or not. If we want to compare the bulk of the energy released with an energy accumulation time, we should be more accurate in defining what we are observing – a single event or a combination of several nanoflares. As we said above, we cannot confidently distinguish between these two scenarios for the event studied.

In addition to the new flux emergence, solar flares are often caused by shear motions of the magnetic footpoints (see, for example, Bogachev *et al.*, 2005). To understand the role of these processes in this particular event, we have applied the Differential Affine Velocity Estimator method (DAVE: Schuck, 2006) to reconstruct the tangential velocity field on the solar surface. The results of the reconstruction are shown in Figure 6. In the center of the flaring region (area of the most intensive energy release), we did not see any appreciable plasma motions that may be the reason behind the nanoflare. Relatively important motions were only observed in the north-eastern part of the region (in the vicinity of flux P1), but they did not result here in any topological changes or energy release.

In order to estimate the free-magnetic energy and 3D distribution of electric currents in the region, we developed and applied a non-linear force-free field (NLFFF) extrapolation, which was based on the method of magnetic friction (Craig and Sneyd, 1986). We started

Figure 7 EUV emission of the nanoflare in the 171 Å AIA channel (*upper panel*) and normalized density of the electric current at the height of 1.5 Mm (*bottom panel*) calculated from NLFFF extrapolation (Craig and Sneyd, 1986).
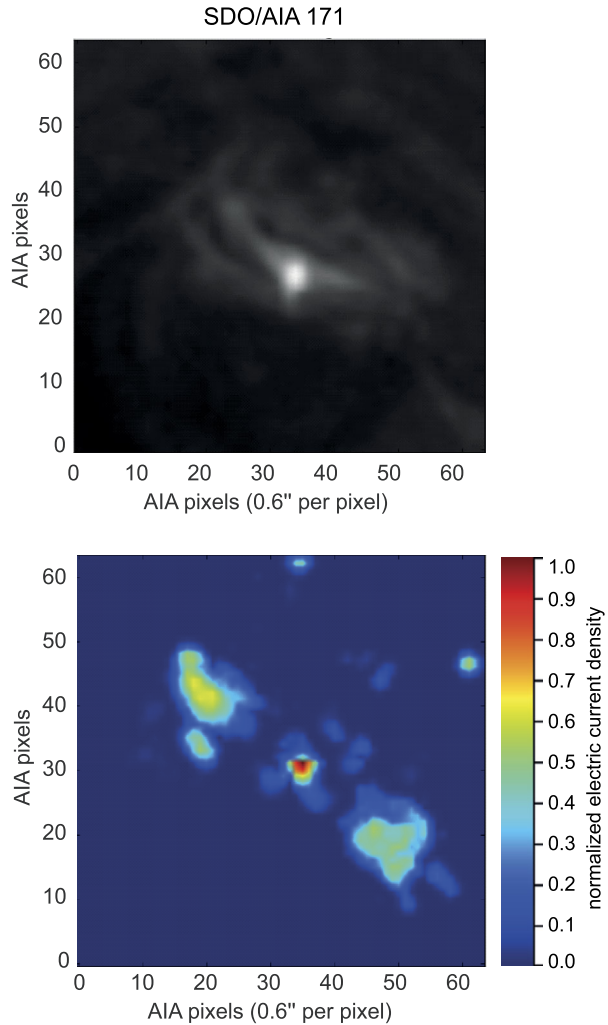
from the initial magnetic configuration at 01:10 UT, which was postulated to be potential, and then studied its transformation by the horizontal component of the photospheric-plasma flows. The velocity values at each step required for calculations were found using the DAVE method. Following this procedure, we first estimated the initial energy of the magnetic configuration before the nanoflare (at 01:10 UT) to be 5.3×10^{27} erg. Then this current-free configuration was transformed step-by-step until the nanoflare maximum at 01:37 UT. The resulting density of electric current in the corona related to this moment is shown in Figure 7. The calculated electric current has a local maximum in the center of the image, which coincides with the region of the most intense EUV emission (see top and bottom panels in Figure 7). Such a coincidence, we think, additionally supports the idea that the energy release during this nanoflare was driven by magnetic reconnection (Somov, 2007; Priest and Forbes, 2007; Somov, 2012).

The amount of free-magnetic energy accumulated between 01:10 UT and 01:37 UT can be found as the difference between the total magnetic energy derived from the NLFFF model

and the initial energy calculated in the potential (current-free) approximation. The NLFFF energy was calculated as in Aly (1989):

$$E_{\mathrm{mag}} = \int_S (x B_x + y B_y) B_z \, \mathrm{d}x \, \mathrm{d}y, \tag{4}$$

where S is the region of integration on the Sun's surface (coinciding with the field of view in Figures 6 and 7). The resulting free energy was found from this to be

$$\Delta E_{\mathrm{mag}} = 8.9 \times 10^{25} \text{ erg.} \tag{5}$$

It can be noted that the excess of free energy accumulated before the nanoflare occurred is only about 1.7% of the potential energy of the magnetic configuration. By comparing the value in Equation 5 with the energy in Equation 2, we can roughly conclude that about two-thirds of the free-magnetic energy was transferred into the plasma heating in this particular event.

4. Discussion

By analyzing AIA and HMI images, we found a compact EUV radiation source, which we identified as a nanoflare and for which we were able to state an evident correlation between the dynamics of magnetic fields and the features of energy release. The source was associated with a group of small magnetic loops of size about 20 Mm, it was located near the top of one of the loops, and it had a temperature of about 3 MK and a lifetime of about ten minutes.

The magnetic configuration in the vicinity of the nanoflare consisted of six nearly isolated magnetic fluxes, three of which were of a positive polarity, and three others that were negative. The nanoflare was triggered by an emergence of a new magnetic flux, labeled in this work as $P3 - N3$, which is easily seen in the HMI magnetograms. Above the solar surface, in the corona, we found four magnetic null-points, two of which were formed by the new flux. Just in the vicinity of these new X-points, the strongest energy release took place. We have not found any other possible triggers of the nanoflare, including shear motions of the plasma. The time interval between the flux emergence and the initial nanoflare was about of $15 - 20$ minutes. We consider this time as the period for energy accumulation, which should precede any flare. The thermal energy released in the nanoflare was estimated as 6×10^{25} erg, which was equal to of about two-thirds of the total free energy accumulated in the region: 9×10^{25} erg. The distribution of the electric currents in the corona calculated in the NLFFF approximation reached its maximum at about 1.5 Mm; this maximum coincided with the region of the most intense energy release.

The event that we studied was one of the largest in the dataset, which explains why we think that the plasma temperature of 3 MK should be considered as an upper limit for nanoflares. By the same reasoning, we think that the energy accumulation time of $15 - 20$ minutes should exceed the average value. On the other hand, this is still significantly faster than the energy storage in larger flares, which can last for several hours (Nitta *et al.*, 1996) to one day or longer (Somov *et al.*, 2002).

Concerning the ratio of two-thirds between the released thermal energy and the free energy amount accumulated in the magnetic field, we are not sure whether this is typical for most nanoflares or not. For normal and large flares, it is known that a significant amount of energy is released in other forms, in particular as the kinetic energy of plasma motions or

in the form of accelerated particles (Aschwanden *et al.*, 2016, 2017). These typical energy releases may also exist in nanoflares but have not been discovered from observations so far.

Disclosure of Potential conflicts of Interest   The authors declare that they have no conflicts of interest.

Publisher's Note   Springer Nature remains neutral with regard to jurisdictional claims in published maps and institutional affiliations.

References

Aly, J.J.: 1989, On the reconstruction of the nonlinear force-free coronal magnetic field from boundary data. *Solar Phys.* **120**, 19. DOI. ADS.

Aschwanden, M.J.: 1999, Do EUV nanoflares account for coronal heating? *Solar Phys.* **190**, 233. DOI. ADS.

Aschwanden, M.J., Holman, G., O'Flannagain, A., Caspi, A., McTiernan, J.M., Kontar, E.P.: 2016, Global energetics of solar flares. III. Nonthermal energies. *Astrophys. J.* **832**, 27. DOI. ADS.

Aschwanden, M.J., Caspi, A., Cohen, C.M.S., Holman, G., Jing, J., Kretzschmar, M., Kontar, E.P., McTiernan, J.M., Mewaldt, R.A., O'Flannagain, A., Richardson, I.G., Ryan, D., Warren, H.P., Xu, Y.: 2017, Global energetics of solar flares. V. Energy closure in flares and coronal mass ejections. *Astrophys. J.* **836**, 17. DOI. ADS.

Barnes, W.T., Cargill, P.J., Bradshaw, S.J.: 2016a, Inference of heating properties from "hot" non-flaring plasmas in active region cores. I. Single nanoflares. *Astrophys. J.* **829**, 31. DOI. ADS.

Barnes, W.T., Cargill, P.J., Bradshaw, S.J.: 2016b, Inference of heating properties from "hot" non-flaring plasmas in active region cores. II. Nanoflare trains. *Astrophys. J.* **833**, 217. DOI. ADS.

Benz, A.O., Grigis, P.C.: 2002, Microflares and hot component in solar active regions. *Solar Phys.* **210**, 431. DOI. ADS.

Benz, A.O., Krucker, S.: 2002, Energy distribution of microevents in the quiet solar corona. *Astrophys. J.* **568**, 413. DOI. ADS.

Bogachev, S.A., Somov, B.V., Kosugi, T., Sakao, T.: 2005, The motions of the hard X-ray sources in solar flares: Images and statistics. *Astrophys. J.* **630**, 561. DOI. ADS.

Craig, I.J.D., Sneyd, A.D.: 1986, A dynamic relaxation technique for determining the structure and stability of coronal magnetic fields. *Astrophys. J.* **311**, 451. DOI. ADS.

Cranmer, S.R.: 2018, Low-frequency Alfvén waves produced by magnetic reconnection in the Sun's magnetic carpet. *Astrophys. J.* **862**, 6. DOI. ADS.

Delaboudinière, J.-P., Artzner, G.E., Brunaud, J., Gabriel, A.H., Hochedez, J.F., Millier, F., Song, X.Y., Au, B., Dere, K.P., Howard, R.A., Kreplin, R., Michels, D.J., Moses, J.D., Defise, J.M., Jamar, C., Rochus, P., Chauvineau, J.P., Marioge, J.P., Catura, R.C., Lemen, J.R., Shing, L., Stern, R.A., Gurman, J.B., Neupert, W.M., Maucherat, A., Clette, F., Cugnon, P., van Dessel, E.L.: 1995, EIT: Extreme-Ultraviolet Imaging Telescope for the SOHO mission. *Solar Phys.* **162**, 291. DOI. ADS.

Georgoulis, M.K., Rust, D.M., Bernasconi, P.N., Schmieder, B.: 2002, Statistics, morphology, and energetics of Ellerman bombs. *Astrophys. J.* **575**, 506. DOI. ADS.

Guerreiro, N., Haberreiter, M., Hansteen, V., Schmutz, W.: 2017, Small-scale heating events in the solar atmosphere. II. Lifetime, total energy, and magnetic properties. *Astron. Astrophys.* **603**, A103. DOI. ADS.

Hoyng, P., Brown, J.C., van Beek, H.F.: 1976, High time resolution analysis of solar hard X-ray flares observed on board the ESRO TD-1A satellite. *Solar Phys.* **48**, 197. DOI. ADS.

Hudson, H.S.: 1991, Solar flares, microflares, nanoflares, and coronal heating. *Solar Phys.* **133**, 357. DOI. ADS.

Kirichenko, A.S., Bogachev, S.A.: 2013, Long-duration plasma heating in solar microflares of X-ray class A1.0 and lower. *Astron. Lett.* **39**, 797. DOI. ADS.

Kirichenko, A.S., Bogachev, S.A.: 2017a, Plasma heating in solar microflares: Statistics and analysis. *Astrophys. J.* **840**, 45. DOI. ADS.

Kirichenko, A.S., Bogachev, S.A.: 2017b, The relation between magnetic fields and X-ray emission for solar microflares and active regions. *Solar Phys.* **292**, 120. DOI. ADS.

Kuzin, S.V., Bogachev, S.A., Zhitnik, I.A., Pertsov, A.A., Ignatiev, A.P., Mitrofanov, A.M., Slemzin, V.A., Shestov, S.V., Sukhodrev, N.K., Bugaenko, O.I.: 2009, TESIS experiment on EUV imaging spectroscopy of the Sun. *Adv. Space Res.* **43**, 1001. DOI. ADS.

Lemen, J.R., Title, A.M., Akin, D.J., Boerner, P.F., Chou, C., Drake, J.F., Duncan, D.W., Edwards, C.G., Friedlaender, F.M., Heyman, G.F., Hurlburt, N.E., Katz, N.L., Kushner, G.D., Levay, M., Lindgren, R.W., Mathur, D.P., McFeaters, E.L., Mitchell, S., Rehse, R.A., Schrijver, C.J., Springer, L.A., Stern, R.A., Tarbell, T.D., Wuelser, J.-P., Wolfson, C.J., Yanari, C., Bookbinder, J.A., Cheimets, P.N., Caldwell, D., Deluca, E.E., Gates, R., Golub, L., Park, S., Podgorski, W.A., Bush, R.I., Scherrer, P.H., Gummin, M.A., Smith, P., Auker, G., Jerram, P., Pool, P., Soufli, R., Windt, D.L., Beardsley, S., Clapp, M., Lang, J., Waltham, N.: 2012, The Atmospheric Imaging Assembly (AIA) on the Solar Dynamics Observatory (SDO). *Solar Phys.* **275**, 17. DOI. ADS.

Longcope, D.W.: 2005, Topological methods for the analysis of solar magnetic fields. *Liv. Rev. Solar Phys.* **2**, 7. DOI. ADS.

Meyer, K.A., Mackay, D.H., van Ballegooijen, A.A.: 2012, Solar magnetic carpet II: Coronal interactions of small-scale magnetic fields. *Solar Phys.* **278**, 149. DOI. ADS.

Nelson, C.J., Doyle, J.G., Erdélyi, R., Huang, Z., Madjarska, M.S., Mathioudakis, M., Mumford, S.J., Reardon, K.: 2013, Statistical analysis of small Ellerman bomb events. *Solar Phys.* **283**, 307. DOI. ADS.

Nitta, N., van Driel-Gesztelyi, L., Leka, K.D., Shibata, K.: 1996, Emerging flux and flares in NOAA 7260. *Adv. Space Res.* **17**, 201. DOI. ADS.

Parker, E.N.: 1988, Nanoflares and the solar X-ray corona. *Astrophys. J.* **330**, 474. DOI. ADS.

Parnell, C.E., Jupp, P.E.: 2000, Statistical analysis of the energy distribution of nanoflares in the quiet Sun. *Astrophys. J.* **529**, 554. DOI. ADS.

Pevtsov, A.A., Fisher, G.H., Acton, L.W., Longcope, D.W., Johns-Krull, C.M., Kankelborg, C.C., Metcalf, T.R.: 2003, The relationship between X-ray radiance and magnetic flux. *Astrophys. J.* **598**, 1387. DOI. ADS.

Priest, E.: 2014, *Magnetohydrodynamics of the Sun*, Cambridge University Press, Cambridge. ADS.

Priest, E.R., Chitta, L.P., Syntelis, P.: 2018, A cancellation nanoflare model for solar chromospheric and coronal heating. *Astrophys. J. Lett.* **862**, L24. DOI. ADS.

Priest, E., Forbes, T.: 2007, *Magnetic Reconnection*, Cambridge University Press, Cambridge. ADS.

Reid, A., Mathioudakis, M., Doyle, J.G., Scullion, E., Nelson, C.J., Henriques, V., Ray, T.: 2016, Magnetic flux cancellation in Ellerman bombs. *Astrophys. J.* **823**, 110. DOI. ADS.

Reva, A., Shestov, S., Bogachev, S., Kuzin, S.: 2012, Investigation of Hot X-Ray Points (HXPs) using spectroheliograph Mg XII experiment data from CORONAS-F/SPIRIT. *Solar Phys.* **276**, 97. DOI. ADS.

Scherrer, P.H., Schou, J., Bush, R.I., Kosovichev, A.G., Bogart, R.S., Hoeksema, J.T., Liu, Y., Duvall, T.L., Zhao, J., Title, A.M., Schrijver, C.J., Tarbell, T.D., Tomczyk, S.: 2012, The Helioseismic and Magnetic Imager (HMI) investigation for the Solar Dynamics Observatory (SDO). *Solar Phys.* **275**, 207. DOI. ADS.

Schuck, P.W.: 2006, Tracking magnetic footpoints with the magnetic induction equation. *Astrophys. J.* **646**, 1358. DOI. ADS.

Shimizu, T., Tsuneta, S.: 1997, Deep survey of solar nanoflares with *Yohkoh*. *Astrophys. J.* **486**, 1045. DOI. ADS.

Somov, B.V.: 2007, *Plasma Astrophysics, Part II: Reconnection and Flares*, Springer, Berlin. ADS.

Somov, B.V.: 2012, On the magnetic reconnection of electric currents in solar flares. *Astron. Lett.* **38**, 128. DOI. ADS.

Somov, B.V., Kosugi, T., Hudson, H.S., Sakao, T., Masuda, S.: 2002, Magnetic reconnection scenario of the Bastille Day 2000 flare. *Astrophys. J.* **579**, 863. DOI. ADS.

Stenflo, J.O.: 1985, Measurements of magnetic fields and the analysis of Stokes profiles. *Solar Phys.* **100**, 189. DOI. ADS.

Watanabe, H., Vissers, G., Kitai, R., Rouppe van der Voort, L., Rutten, R.J.: 2011, Ellerman bombs at high resolution. I. Morphological evidence for photospheric reconnection. *Astrophys. J.* **736**, 71. DOI. ADS.